

XMM-Newton first X-ray detection of the LoBAL quasar PG 1700+518

L. Ballo¹, E. Piconcelli², C. Vignali³, and N. Schartel⁴

¹*Instituto de Física de Cantabria (CSIC-UC), Avda. Los Castros s/n (Edif. Juan Jordá), E-39005 Santander (Spain); ballo@ifca.unican.es*

²*Osservatorio Astronomico di Roma (INAF), via Frascati 33, I-00040 Monteporzio Catone, Roma, (Italy)*

³*Dipartimento di Astronomia, Università degli Studi di Bologna, via Ranzani 1, I-40127, Bologna, (Italy)*

⁴*XMM-Newton Science Operation Centre, ESAC, ESA, P.O. Box 78, E-28691 Villanueva de la Cañada, Madrid, (Spain)*

Accepted 2011 April 8. Received 2011 April 6; in original form 2011 March 4

ABSTRACT

We report the first high-energy detection of PG 1700+518, a well-known low-ionization broad absorption line quasar (QSO). Due to previous X-ray non-detection, it was classified as soft X-ray weak QSO. We observed PG 1700+518 with XMM-Newton for about 60 ksec divided in three exposures. The spectrum below 2 keV is very steep, $\Gamma \sim 2.4 - 3.8$, while at higher energies the extremely flat emission (photon index $\Gamma \sim 0.15$, when modelled with a power law) suggests the presence of strong absorption ($N_{\text{H,pl}} \sim 2 \times 10^{23} \text{ cm}^{-2}$, Γ fixed to 1.8), or a reflection-dominated continuum. The broad-band flux is consistent with previous non-detection. Simultaneous EPIC and OM data confirm its X-ray weakness (*observed* $\alpha_{\text{ox}} \sim -2.2$). The level of obscuration derived from the X-ray spectra of PG 1700+518 cannot explain its soft X-ray nuclear weakness unless a column density of $N_{\text{H}} \gtrsim 2 \times 10^{24} \text{ cm}^{-2}$ is present.

Key words: galaxies: active – quasars: individual: PG 1700+518 – X-rays: galaxies

1 INTRODUCTION

The so-called “soft X-ray weak QSOs” (SXWQs, X-ray-to-optical spectral index $\alpha_{\text{ox}} \equiv \log(F_{2\text{keV}}/F_{2500\text{\AA}})/\log(\nu_{2\text{keV}}/\nu_{2500\text{\AA}}) \lesssim -2$, Laor et al. 1997; $\sim 10\%$ of nearby PG QSOs, Brandt, Laor, & Wills 2000) are active galactic nuclei (AGN) notably faint in X-rays relative to their optical/UV fluxes. Recently, Gibson, Brandt, & Schneider (2008), studying the frequency of intrinsically SXWQs in optically selected samples, found that [excluding Broad Absorption Line (BAL)] $\lesssim 2\%$ SDSS QSOs are genuinely X-ray weak.

Several possible explanations of this weakness have been proposed over the past years, all related to the X-ray band (the optical-UV flux in the SXWQs is not strongly variable and, therefore, it is difficult to ascribe the X-ray weakness to a temporary high emission state at these wavelengths). The presence of absorbers (neutral or partially ionized) can reduce in a considerable way the observed high-energy emission (Gallagher et al. 2001, 2005; Piconcelli et al. 2005; see e.g. Q1246-057 and SBS1542+541, Grupe, Mathur, & Elvis 2003; Mrk 304, Piconcelli et al. 2004; WPVS 007, Grupe et al. 2007; Grupe, Leighly, & Komossa 2008; Mrk 335, Grupe et al. 2008; PG 1535+547, Ballo et al. 2008). Strong UV absorption features of SXWQs classified as BAL sources are known to be related to warm absorbers (Crenshaw, Kraemer, & George 2003). Significant correlations have also been found between the degree of X-ray weakness (i.e., how the L_{X} differ from that expected for a typical QSO having the same L_{UV} ; e.g., Gibson, Brandt, & Schneider 2008, and

references therein) and acceleration-dependent BAL properties in the BAL QSOs belonging to the SDSS (Gibson et al. 2009). A strong variability of the intrinsic X-ray continuum can be another reason of weakness at high energies. In this case, the classification as SXWQ is based on observations performed during a low emission state of the source (see e.g. PG 0844+349, Gallo et al. 2011, and references therein; 1H 0419-577, Pounds et al. 2004; Mrk 335, Grupe, Komossa, & Gallo 2007). In this scenario, a reflection-dominated continuum originating in the accretion disc (caused by strong light bending) can also play an important role (see Schartel et al. 2007, 2010; Gallo et al. 2011). Finally, the observed weakness can be an intrinsic property, due to a fundamentally distinct emission mechanism (Risaliti et al. 2003; see also the case of PG 1254+047, Sabra & Hamann 2001; PHL 1811, Leighly et al. 2007). This last hypothesis implies different scenarios for the accretion disc. Higher accretion rates can produce a steeper α_{ox} if the X-ray photons are emitted in a more central region than the UV-optical photons (Zdziarski & Gierliński 2004), or via the so-called “photon-trapping” (Begelman & Rees 1978; Kawaguchi 2003). Another possibility is that the corona is radiatively inefficient (e.g., Bechtold et al. 2003; Proga 2005). The most likely explanation for the dramatic steepening of α_{ox} reported by Miniutti et al. (2009) for PHL 1092 seems to be a transient dramatic weakening or disruption of the X-ray corona.

PG 1700+518 ($z = 0.292$; Schmidt & Green 1983) is the most luminous radio-quiet QSO in the optically selected PG sample (absolute magnitude $M_{\text{B}} = -25.2$; Véron-Cetty & Véron 2010). The

source resides in a system composed by two apparently interacting galaxies, with widely separated nuclei ($\sim 1.6''$, corresponding to ~ 7 kpc at the source redshift; e.g., Guyon, Sanders, & Stockton 2006). Observational evidences are consistent with the companion being a collisional ring galaxy, possibly produced by a near head-on collision with the QSO host. The IR luminosity $L_{8-1000\mu\text{m}} \sim 5.5 \times 10^{12} L_{\odot}$ (estimated from *IRAS*, *ISO*, and *Spitzer* data; Evans et al. 2009) implies for the whole system a classification as Ultra-Luminous Infrared Galaxy. A rough indication for the bolometric luminosity, $L_{\text{bol}} \sim 2.7 \times 10^{46}$ ergs s^{-1} , was obtained by Evans et al. (2009) from this L_{IR} (adopting a ratio $L_{\text{IR}}/L_{0.1-1\mu\text{m}} = 0.76$; Guyon, Sanders, & Stockton 2006); given the black hole mass of $M_{\text{BH}} = 7.81 \times 10^8 M_{\odot}$ (Peterson et al. 2004), this implies a quite large Eddington ratios, $L_{\text{bol}}/(1.3 \times 10^{38} M_{\text{BH}}) \sim 0.27$, as expected for this kind of sources. Assuming that the luminosity in the far-IR corresponds to the luminosity of the starburst (SB), a star formation rate for the QSO host of $SFR \sim 210 M_{\odot} \text{yr}^{-1}$ is estimated (Evans et al. 2009). Millimetre-wave CO(1 \rightarrow 0) observations allow the authors to derive for the system a molecular gas mass of $M_{\text{H}_2} \sim 5.7 \times 10^{10} M_{\odot}$ (mainly associated with the QSO host), converting it into one of the most molecular gas-rich PG QSO host systems. Moreover, PG 1700+518 belongs to the rare class of low-ionization broad absorption line (loBAL) QSOs, a very rare subclass ($\sim 10\%$) of BAL QSOs showing absorption from both low- and high-ionization species.

At high energies, *ROSAT* and *ASCA* non-detections are the only X-ray information collected so far (Green & Mathur 1996; Gallagher et al. 1999; Brandt, Laor, & Wills 2000; George et al. 2000). A power-law (PL) model with $\Gamma = 2$ implies an *ASCA* $F_{2-10\text{keV}} < 8 \times 10^{-14}$ ergs $\text{cm}^{-2} \text{s}^{-1}$ (George et al. 2000). From the 3σ upper limit to the *ROSAT* rate ($< 3.4 \times 10^{-3}$ counts s^{-1} , up to ~ 2.5 keV), Green & Mathur (1996) estimated an index $\alpha_{\text{ox}} < -2.30$. With optical spectropolarimetric studies of the broad Balmer H α and H β emission lines, Young et al. (2007) demonstrate the presence of a wind launched from a relatively narrow annulus within the accretion disc of PG 1700+518. The two-zones wind model adopted by the authors to interpret the observations can explain observed properties such as BALs and X-ray absorbers. Indeed, it requires the presence of an inner self-shielding region, opaque to X-rays. On the other hand, the BALs should be formed in a part of the wind different from the X-ray-absorbing zone, arising in the shielded outer wind. This wind can be responsible for the extinction of an intrinsically normal X-ray emission.

In this paper we present the analysis of our *XMM-Newton* observation of PG 1700+518, providing the first X-ray detection of this SXWQ. In our analysis, we assume a cosmology with $\Omega_{\text{M}} = 0.3$, $\Omega_{\Lambda} = 0.7$, and $H_0 = 70 \text{ km s}^{-1} \text{ Mpc}^{-1}$, implying a luminosity distance of $D_{\text{L}} \approx 1505 \text{ Mpc}$. All literature measurements have been converted to this cosmology.

2 OBSERVATION AND DATA REDUCTION

XMM-Newton (Jansen et al. 2001) observed PG 1700+518 (RA=17^h01^m24.8^s, Dec=+51^d49^m20^s) in December 2009/January 2010, for about 60 ksec divided in three exposures, the first separated by about two weeks from the others (Obs. ID 0601870101, 0601870201, and 0601870301; hereafter, 101, 201, and 301, respectively). The observations were performed with the European Photon Imaging Camera (EPIC; pn, Strüder et al. 2001; MOS, Turner et al. 2001), the Optical Monitor (OM; Mason et al. 2001) and the Reflection Grating Spectrometer; the source is not

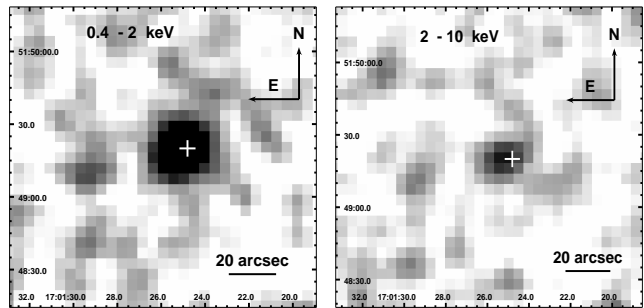


Figure 1. The 0.4 – 2 keV (*left*) and 2 – 10 keV (*right*) EPIC images (pn, MOS1, and MOS2 for observations 101, 201, and 301 combined) of PG 1700+518, smoothed with a Gaussian function with kernel radius of 2. The white cross marks the optical position of the QSO.

detected with the last instrument. The three EPIC cameras were operating in full frame mode, with the thin filter applied. OM performed observations with the UVW1 ($\lambda_{\text{eff}} = 2910 \text{ \AA}$) and UVM2 ($\lambda_{\text{eff}} = 2310 \text{ \AA}$) filters in the optical light path; all OM exposures were performed in the default image mode.

The data have been processed following the standard procedures, using the Science Analysis Software (SAS version 10.0.2) with calibration from July 2010. EPIC event files have been filtered for high-background time intervals, following the standard method consisting in rejecting periods of high count rate at energies > 10 keV. The net exposure times at the source position after data cleaning are ~ 9 , 16, and 19 ks (MOS1), ~ 15 , 17, and 18 ks (MOS2), and ~ 4 , 9, and 15 ks (pn). Figure 1 shows the EPIC images obtained combining event files from all cameras for the three exposures in the 0.4 – 2 keV (*left panel*) and 2 – 10 keV (*right panel*) energy ranges (the white cross marks the optical position of PG 1700+518). The source is detected with a 0.5 – 2 keV EPIC detection likelihood above 5 in all the observations (according to the results of the SAS task *edetect_chain* applied to the cleaned data); above 2 keV, there is no detection in the observation 101 (as well as in the MOS1 data of the 201), while the source is marginally detected in the three cameras during the observation 301, and in the pn and MOS2 data of the 201 (see Table 1).

We extracted source counts from a circular region of $15''$ radius, enclosing both the QSO host and the galaxy companion; background counts were extracted from a source-free circular region in the same chip of $30''$ radius. In Table 1 we report the net count rates and signal-to-noise ratios (S/N) in the 0.4 – 2 keV and 2 – 10 keV observed energy ranges, corresponding to 0.5 – 2.6 keV and 2.6 – 12.9 keV in the frame of the source. No statistically significant variability has been detected during each observation. In Table 2 we compare the observed variance, as evaluated from the data scatter, to the variance expected from a constant source, as evaluated from the errors in the count rates. This is done for background-subtracted data in bins of 500 sec each. Given the relatively high black hole mass of PG 1700+518, we note that even the longer exposure (after cleaning) is less than 3 times the crossing time $t_{\text{cross}} \equiv R_{\text{g}}/c \sim 7700$ sec. Therefore, we do not expect variability in a single observation.

For each observation, we obtained two images for each OM filter. The count rate information was averaged; the resulting AB magnitudes are: in the UVM2 filter, 16.01 ± 0.01 , 16.00 ± 0.01 , and 16.00 ± 0.01 ; in the UVW1 filter, 15.70 ± 0.01 , 15.67 ± 0.01 , and 16.68 ± 0.01 (for observations 101, 201, and 301, respectively).

than expected from a $SFR \sim 210 M_{\odot} \text{ yr}^{-1}$, (as estimated by Evans et al. 2009 assuming that L_{FIR} is the SB luminosity). According to Ranalli, Comastri, & Setti (2003), the soft X-ray luminosity corresponding to this SFR is indeed $L_{0.5-2 \text{ keV}, SFR} \sim 10^{42} \text{ ergs s}^{-1}$. A contribution from the AGN is likely present at the mid-IR/FIR wavelengths which are used in the estimate of the SFR ; therefore, this value can be assumed as an upper limit to the soft X-ray luminosity expected from the SB. The present data do not allow to disentangle the SB-related from the AGN-related X-ray emission leaving free to vary all the parameters of interest; however, we can investigate the relative contribution of AGN and SB by fixing the intensity of the latter to the expected upper limit. Residuals are well modelled by a power law flatter than previously found but still consistent, given the large associated uncertainties, $\Gamma = 2.4^{+1.6}_{-1.1}$, with a luminosity $L_{0.4-2 \text{ keV}, PL} = 3.1^{+5.7}_{-1.7} \times 10^{42} \text{ ergs s}^{-1}$; the parameters are poorly constrained, with $N_{\text{H}} = 1.2^{+2.5}_{-1.0} \times 10^{21} \text{ cm}^{-2}$ and $kT = 0.7^{+0.4}_{-0.3} \text{ keV}$ ($C/\text{d.o.f.} = 141.3/175$).

When extended to the whole energy range, strong residuals at high energy are clearly evident (see Fig. 2, *lower panel*). A simple power law fitted to the data above 2 keV results to be extremely flat, $\Gamma = 0.2^{+0.8}_{-0.9}$, leaving a strong soft excess below 2 keV.

Such an extremely flat power law suggests the presence of absorption, or it can be interpreted as a reflection component. We tested both hypotheses (i.e., transmission vs. reflection-dominated scenarios), adopting for the latter the `PEXRAV` model in `XSPEC` (Magdziarz & Zdziarski 1995). The statistic quality of the data above $\sim 3 \text{ keV}$ is too low to constrain at the same time all the spectral parameters for the reflection component or the high-energy absorbed power law; in the following, we fix the photon index of the intrinsic nuclear emission to a typical value for unabsorbed AGN, $\Gamma = 1.8$ (e.g., Piconcelli et al. 2005; Mateos et al. 2010). Both the adopted models are adequate to describe the overall broad-band shape, with values for the common model parameter, the soft-component photon index, consistent within the errors: $\Gamma_{\text{soft}} = 4.5^{+1.3}_{-1.1}$ and $3.9^{+1.3}_{-0.9}$, when a reflection-dominated continuum or a transmission scenario are assumed, respectively. A fit with an absorbed power law implies a high column density of $N_{\text{H}, pl} = 2.4^{+4.0}_{-1.7} \times 10^{23} \text{ cm}^{-2}$. Furthermore, an additional absorption of $N_{\text{H}} = 4.2^{+2.5}_{-2.1} \times 10^{21} \text{ cm}^{-2}$ and $3.4^{+2.4}_{-1.9} \times 10^{21} \text{ cm}^{-2}$, depending on the continuum model, covering both spectral components, is also required. From a statistical point of view, at high energy a transmission or a reflection-dominated model are indistinguishable ($C = 262.5$ for 290 d.o.f. vs. 262.2 for 291 d.o.f.); the low S/N prevents us from completely ruling out any possibility.

When the expected soft contribution from SB is included in the model, $L_{0.5-2 \text{ keV}, \text{MEKAL}} \sim 10^{42} \text{ ergs s}^{-1}$, we found a flatter soft AGN-related power law, $\Gamma_{\text{soft}} = 1.9 \pm 0.5$ and 2.0 ± 0.6 for the transmission or the reflection-dominated scenario, respectively. In the former case, the absorber covering the intrinsic nuclear power law has a column density $N_{\text{H}, pl} = 6.1^{+51.9}_{-1.5} \times 10^{23} \text{ cm}^{-2}$. The additional absorption covering the all the spectral components is no longer required ($\Delta C/\text{d.o.f.} = 2.0/1$ and $3.0/1$); the two scenarios are still indistinguishable ($C = 259.5$ for 290 d.o.f. vs. $C = 261.6$ for 291 d.o.f.).

In principle, the equivalent width of the Fe $K\alpha$ line can help in discriminating between a transmission or a reflection-dominated origin of the high-energy emission, but this feature is not detected. No meaningful upper limit for the line equivalent width can be obtained, due to the high background, dominating above 2 keV (see Fig. 3).

For an high-energy absorbed power-law model, we measure a total 0.4–2 keV [2–10 keV] flux (corrected for Galactic absorption)

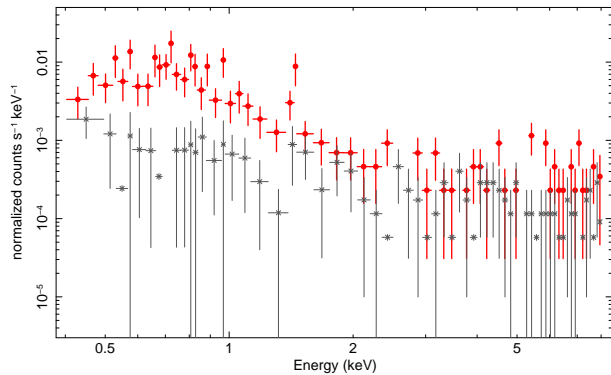


Figure 3. Source plus background pn spectrum (red filled circles), for the three observations combined, compared with the background (black crosses). For graphical purposes, data have been binned to a 2σ significance.

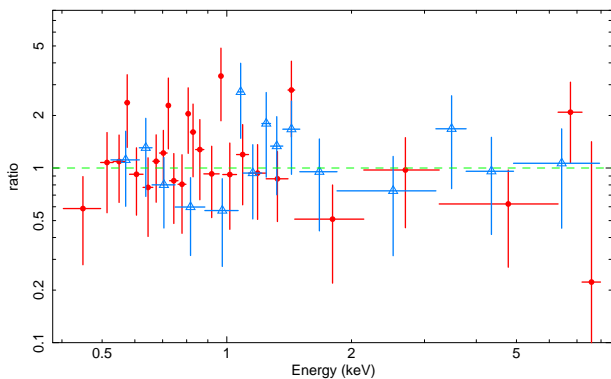


Figure 4. Background-subtracted data-to-model ratio for the pn (red filled circles) and MOS (blue open triangles) for the transmission scenario. The fitting model consists of an absorbed power law, an unabsorbed power law, and a `MEKAL` thermal emission component (with fixed intensity, see text). For graphical purposes, data have been binned to a 2σ significance.

of $9.7^{+10.6}_{-4.5} \times 10^{-15} \text{ ergs cm}^{-2} \text{ s}^{-1}$ [$1.84^{+2.69}_{-0.99} \times 10^{-14} \text{ ergs cm}^{-2} \text{ s}^{-1}$]. The total luminosity in the hard band is $L_{2-10 \text{ keV}} = 1.0^{+1.5}_{-0.5} \times 10^{43} \text{ ergs s}^{-1}$. When the SB contribution is included, as a thermal component with $L_{0.5-2 \text{ keV}, \text{MEKAL}} \sim 10^{42} \text{ ergs s}^{-1}$, the hard X-ray luminosity associated with the obscured power-law continuum, representing the primary AGN emission in the transmission scenario, is $L_{2-10 \text{ keV}, PL} \sim 1.3 \times 10^{43} \text{ ergs s}^{-1}$. Data-to-model ratio for this spectral fit is shown in Figure 4.

Finally, the total observed 0.4 – 10 keV flux measured with *XMM-Newton*, $2.72^{+3.65}_{-1.39} \times 10^{-14} \text{ ergs cm}^{-2} \text{ s}^{-1}$, is consistent with the upper limit in the 0.6 – 10 keV *ASCA* SIS0 counts reported by George et al. (2000), i.e. $< 3 \times 10^{-3} \text{ counts s}^{-1}$: assuming the steep power law+absorbed power law model best fitting the *XMM-Newton* data, `WEBSPEC`² predicts an *ASCA* SIS0 count rate between 0.6 and 9.5 keV of $\sim 0.87 \times 10^{-3} \text{ counts s}^{-1}$.

4 DISCUSSION AND CONCLUSIONS

We have presented the first X-ray detection of the *loBAL* SXWQ PG 1700+518, obtained from our *XMM-Newton* observations. Most of the flux is emitted below 2 keV; above this energy, the

² See <http://heasarc.gsfc.nasa.gov/webspec/webspec.html>

signal is weak (see Fig. 3). The observed flux is consistent with previous *ASCA* non-detection in this source.

The soft emission is well described by a steep power law with $\Gamma \sim 3.8$, or assuming a thermal component with $kT \sim 0.6$ keV. However, the luminosity derived for this component is a factor of 20 higher than expected from the *SFR*, and suggests that the emission is mainly due to reprocessing of the AGN emission (e.g., Guainazzi & Bianchi 2007), with a contribution due to the SB activity. When the thermal emission is rescaled to the upper limit estimated on the basis of the *SFR*, the lower limit to the AGN contribution to the soft X-ray emission, represented by a power law with $\Gamma \sim 2.4$, is $L_{0.4-2\text{ keV, PL}} \sim 3 \times 10^{42}$ ergs s^{-1} . Above 2 keV, the extremely flat power law ascribed to the AGN can be due to both an high-absorbed power law ($N_{\text{H, pl}} \sim 2 \times 10^{23}$ cm^{-2} , Γ fixed to 1.8) in a transmission scenario, or to a reflection-dominated continuum. While a strong absorption is not unexpected due to the loBAL nature of PG 1700+518, the quality of the data is too low to discriminate between these possibilities, or to constrain more physical models: e.g., to test the ionization state of the absorbing gas (taking into account the BAL nature of this QSO), or to investigate where the hypothetical reflection could take place: distant obscuring matter, implying a Compton-thick nature, or the accretion disk, possibly contributing to the observed soft excess (as in the case of PG 2112+059, Schartel et al. 2007, 2010, or PG 0844+349, Gallo et al. 2011).

No conclusive result is obtained considering the AGN-dominated mid-IR continuum, that can provide an absorption-independent measure of the intrinsic luminosity even for Compton-thick sources. Assuming the $L_{5-6\mu\text{m}} \sim 1.2 \times 10^{45}$ ergs s^{-1} reported by Shi et al. (2007), the absorption-corrected $L_{2-10\text{ keV}} \sim 1.3 \times 10^{43}$ ergs s^{-1} for the power-law component would be consistent (taking into account the strong uncertainties) with both Compton-thin and Compton-thick nature (see e.g. fig. 4 in Alexander et al. 2008). Note that, at face value, from the low luminosity obtained considering a simple power-law model, $L_{2-10\text{ keV}} \sim 2.5 \times 10^{42}$ ergs s^{-1} , PG 1700+518 would lie in the region where Compton-thick sources are expected, in the same diagnostic diagram, thus reinforcing the hypothesis of strong obscuration. Insight into AGN energetics can be obtained from mid-IR emission-line diagnostics. The low ratio between high- and low-ionization line observed in PG 1700+518, $[\text{Ne Romanv}]/[\text{Ne Romanii}] \leq 0.2$ (Evans et al. 2009), typical of energetically weak AGN, is similar to the value observed in the loBAL QSO Mrk 231 ($[\text{Ne Romanv}]/[\text{Ne Romanii}] \leq 0.15$, Armus et al. 2007), where a Compton-thick absorber (Braitto et al. 2004) is able to block the majority of the $[\text{Ne Romanv}]$ line. Non-detection of polycyclic aromatic hydrocarbon (PAH) features in the *Spitzer* IRS spectrum (Shi et al. 2007) of PG 1700+518 can be due to a combination of a mid-IR AGN emission partially sweeping away the PAH, and a not strong contribution from star formation activity: note that Mrk 231, where aromatic features, although weak, are observed (Armus et al. 2007), has a *SFR* $\sim 470 M_{\odot} \text{ yr}^{-1}$ (Farrah et al. 2003), twice the value found for PG 1700+518. Summarizing, mid-IR data are not able to distinguish between an absorbed AGN and a Compton-thick AGN scenarios.

We can use the OM observations with the UV filters to characterize the low-energy emission and to construct a broadband spectral energy distribution (SED) of PG 1700+518 from *simultaneous* UV and X-ray data (in principle, variability can change the classification as SXWQ). The OM flux is compatible, within the errors, with previous observations: in Figure 5 the

OM data (red squares) are overplotted to *HST-FOS*³ and *IUE*⁴ spectra (dotted lines). At higher energies, the EPIC pn data (red open circles) are plotted. From the OM and EPIC data (corrected for Galactic absorption, following the extinction curve provided by Cardelli, Clayton, & Mathis 1989), we compute an observed $\alpha_{\text{ox}} = -2.19 \pm 0.05$. From the relations between the broadband spectral index and the optical luminosities obtained for samples of optically-selected AGN (e.g., Gibson, Brandt, & Schneider 2008, and references therein), we would expect from the L_{UV} of PG 1700+518 a value of $\alpha_{\text{ox}} = -1.59 \pm 0.16$ (where the uncertainty represents the dispersion in the $\alpha_{\text{ox}} - L_{\text{UV}}$ relation); this would imply the X-ray emission marked with the dotted line in Figure 5. This supports the hypothesis of soft X-ray weakness for PG 1700+518.

The observed α_{ox} is typical of optically-selected BAL QSOs ($\alpha_{\text{ox}} \sim -2.5$ - -2, Gallagher et al. 2006; Green & Mathur 1996), while it is more negative than the values found by Giustini, Cappi, & Vignali (2008) for a sample of X-ray selected BAL QSOs (consistent, within the errors, with the index expected from the correlation with L_{UV}). We obtain a low α_{ox} value, i.e. $\alpha_{\text{ox}} = -2.01 \pm 0.20$, even if we consider the absorption-corrected value of the AGN-related luminosity at 2 keV (dashed line in Fig. 5). This means that, although the strong absorption observed in the source (typical of both SXWQs and BAL QSOs) can be partially responsible of the observed low α_{ox} , its effect is not enough to completely explain the soft X-ray weakness of the source. A similar result was found for PG 1254+047, that is not only an intrinsically X-ray weak BAL QSO, like PG 1700+518, but also heavily X-ray absorbed, with a $N_{\text{H}} \geq 2 \times 10^{23}$ cm^{-2} ionized absorber (Sabra & Hamann 2001). On the other hand, the column density required to obtain the expected $\alpha_{\text{ox}} \sim -1.59$ (after correcting for absorption) is consistent with a Compton-thick scenario, $N_{\text{H}} \sim 1.5 \times 10^{24}$ cm^{-2} .

PG 1700+518 is therefore a very peculiar source, thanks to the simultaneous presence of outflowing wind produced in the innermost regions (Young et al. 2007), high nuclear obscuration, and strong star formation activity. These properties make this system similar to Mrk 231, for which Feruglio et al. (2010) provided direct observational evidence of QSO-driven feedback on the host-galaxy gas content. The host galaxy of PG 1700+518 is part of a collisionally interacting system, that is also one of the most molecular gas-rich PG QSO hosts observed to date. This could suggest that also in PG 1700+518 we are observing an early dust-enshrouded phase in the QSO evolution, predicted by the theoretical models of QSO activation by galaxy interactions (Di Matteo, Springel, & Hernquist 2005). Deeper X-ray observations are needed, to properly describe the observed emission, to determine the physical origin of the different components, and to weight the contribution of AGN and SB. Moreover, information on possible variability in spectral shape and/or intensity is fundamental to investigate the nature of the X-ray weakness of PG 1700+518.

ACKNOWLEDGMENTS

We warmly thank the referee, for her/his constructive comments that significantly improved the paper. Based on observations obtained with XMM-Newton (an ESA science mission with instruments and contributions directly funded by ESA Member States

³ See <http://archive.stsci.edu/>.

⁴ See <http://sdc.laef.inta.es/ines/index2.html>

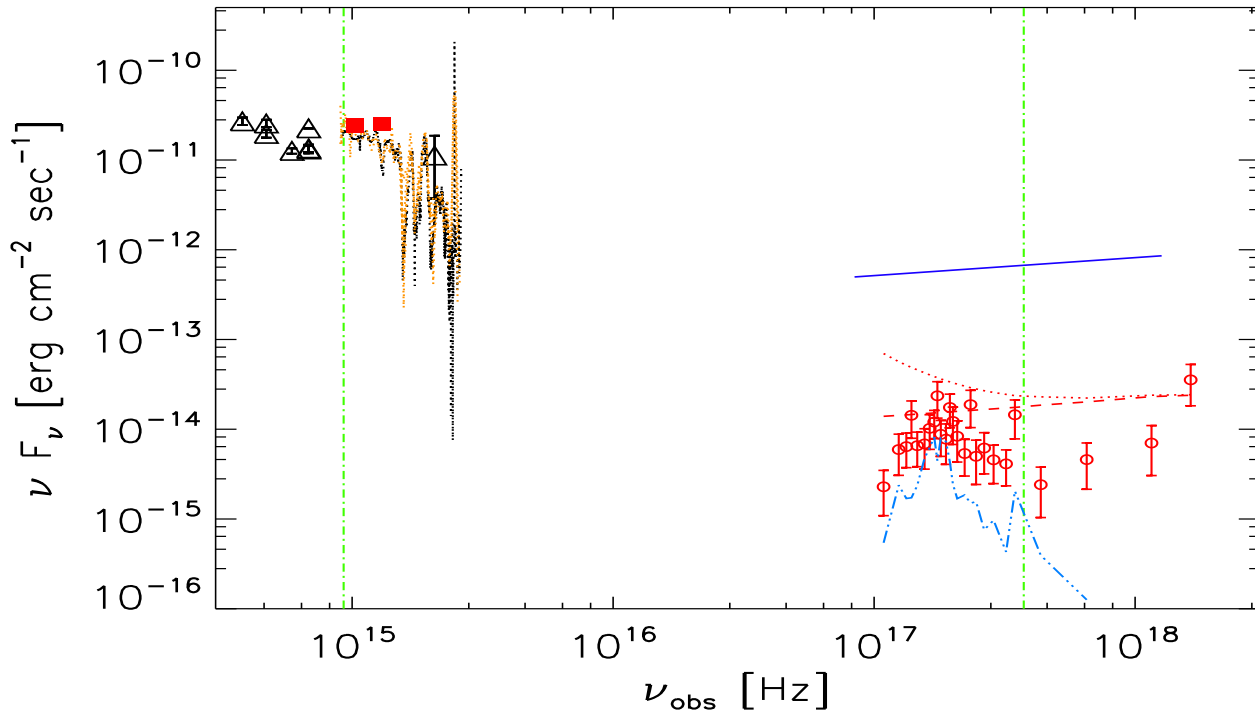


Figure 5. Spectral energy distribution for PG 1700+518. The vertical lines mark $\lambda_{rf} = 2500 \text{ \AA}$ and $E_{rf} = 2 \text{ keV}$. XMM-Newton data: filled squares, OM; open circles, observed XMM-Newton pn flux, binned to a 2σ significance for graphical purposes. Red dotted and dashed lines represent the whole emission and the hard power-law component alone, both unabsorbed, while the light blue dot-dot-dashed curve represents the expected SB emission. The blue solid line indicates the X-ray flux (power law with $\Gamma = 1.8$) expected from OM data assuming an $\alpha_{ox} = -1.59$, typical for QSOs with the L_{UV} of PG 1700+518 (Gibson, Brandt, & Schneider 2008). At lower energies, we show HST-FOS (black dotted line) and IUE (yellow dotted line) spectra. Open triangles are optical data from NED.

and the USA, NASA). LB acknowledges support from the Spanish Ministry of Science and Innovation through a “Juan de la Cierva” fellowship. Financial support for this work was provided by the Spanish Ministry of Science and Innovation, through research grant AYA2009-08059. Support from the Italian Space Agency is acknowledged by EP (contract ASI/INAF I/088/06/0) and CV (contracts I/088/06/0 and I/009/10/0).

REFERENCES

- Alexander D. M., et al., 2008, *ApJ*, 687, 835
 Armus L., et al., 2007, *ApJ*, 656, 148
 Arnaud K. A., 1996, *ASPC*, 101, 17
 Ballo L., Giustini M., Schartel N., Cappi M., Jiménez-Bailón E., Piconcelli E., Santos-Lleo M., Vignali C., 2008, *A&A*, 483, 137
 Bechtold J., et al., 2003, *ApJ*, 588, 119
 Begelman M. C., Rees M. J., 1978, *MNRAS*, 185, 847
 Bianchi S., Guainazzi M., Chiaberge M., 2006, *A&A*, 448, 499
 Braito V., et al., 2004, *A&A*, 420, 79
 Brandt W. N., Laor A., Wills B. J., 2000, *ApJ*, 528, 637
 Cardelli J. A., Clayton G. C., Mathis J. S., 1989, *ApJ*, 345, 245
 Cash W., 1979, *ApJ*, 228, 939
 Crenshaw D. M., Kraemer S. B., George I. M., 2003, *ARA&A*, 41, 117
 Di Matteo T., Springel V., Hernquist L., 2005, *Natur*, 433, 604
 Evans A. S., et al., 2009, *AJ*, 138, 262
 Farrah D., Afonso J., Efstathiou A., Rowan-Robinson M., Fox M., Clements D., 2003, *MNRAS*, 343, 585
 Feruglio C., Maiolino R., Piconcelli E., Menci N., Aussel H., Lamastra A., Fiore F., 2010, *A&A*, 518, L155
 Gallagher S. C., Brandt W. N., Sambruna R. M., Mathur S., Yamasaki N., 1999, *ApJ*, 519, 549
 Gallagher S. C., Brandt W. N., Laor A., Elvis M., Mathur S., Wills B. J., Iyomoto N., 2001, *ApJ*, 546, 795
 Gallagher S. C., Schmidt G. D., Smith P. S., Brandt W. N., Chartas G., Hylton S., Hines D. C., Brotherton M. S., 2005, *ApJ*, 633, 71
 Gallagher S. C., Brandt W. N., Chartas G., Priddey R., Garmire G. P., Sambruna R. M., 2006, *ApJ*, 644, 709
 Gallo L. C., Grupe D., Schartel N., Komossa S., Miniutti G., Fabian A. C., Santos-Lleo M., 2011, *MNRAS*, 412, 161
 George I. M., Turner T. J., Yaqoob T., Netzer H., Laor A., Mushotzky R. F., Nandra K., Takahashi T., 2000, *ApJ*, 531, 52
 Gibson R. R., Brandt W. N., Schneider D. P., 2008, *ApJ*, 685, 773
 Gibson R. R., et al., 2009, *ApJ*, 692, 758
 Giustini M., Cappi M., Vignali C., 2008, *A&A*, 491, 425
 Green P. J., Mathur S., 1996, *ApJ*, 462, 637
 Grupe D., Mathur S., Elvis M., 2003, *AJ*, 126, 1159
 Grupe D., Schady P., Leighly K. M., Komossa S., O’Brien P. T., Nousek J. A., 2007a, *AJ*, 133, 1988
 Grupe D., Komossa S., Gallo L. C., 2007b, *ApJ*, 668, L111
 Grupe D., Komossa S., Gallo L. C., Fabian A. C., Larsson J., Pradhan A. K., Xu D., Miniutti G., 2008, *ApJ*, 681, 982
 Grupe D., Leighly K. M., Komossa S., 2008, *AJ*, 136, 2343
 Guainazzi M., Bianchi S., 2007, *MNRAS*, 374, 1290
 Guyon O., Sanders D. B., Stockton A., 2006, *ApJS*, 166, 89
 Jansen F., et al., 2001, *A&A*, 365, L1

- Kalberla P. M. W., Burton W. B., Hartmann D., Arnal E. M., Bajaja E., Morras R., Pöppel W. G. L., 2005, *A&A*, 440, 775
- Kawaguchi T., 2003, *ApJ*, 593, 69
- Laor A., Fiore F., Elvis M., Wilkes B. J., McDowell J. C., 1997, *ApJ*, 477,
- Leighly K. M., Halpern J. P., Jenkins E. B., Grupe D., Choi J., Prescott K. B., 2007, *ApJ*, 663, 103
- Magdziarz P., Zdziarski A. A., 1995, *MNRAS*, 273, 837
- Mason K. O., et al., 2001, *A&A*, 365, L36
- Mateos S., et al., 2010, *A&A*, 510, A35
- Miniutti G., Fabian A. C., Brandt W. N., Gallo L. C., Boller T., 2009, *MNRAS*, 396, L85
- Peterson B. M., et al., 2004, *ApJ*, 613, 682
- Piconcelli E., Jimenez-Bailón E., Guainazzi M., Schartel N., Rodríguez-Pascual P. M., Santos-Lleó M., 2004, *MNRAS*, 351, 161
- Piconcelli E., Jimenez-Bailón E., Guainazzi M., Schartel N., Rodríguez-Pascual P. M., Santos-Lleó M., 2005, *A&A*, 432, 15
- Pounds K. A., Reeves J. N., Page K. L., O'Brien P. T., 2004, *ApJ*, 605, 670
- Proga D., 2005, *ApJ*, 630, L9
- Ptak A., Serlemitsos P., Yaqoob T., Mushotzky R., 1999, *ApJS*, 120, 179
- Ranalli P., Comastri A., Setti G., 2003, *A&A*, 399, 39
- Reeves J., Done C., Pounds K., Terashima Y., Hayashida K., Anabuki N., Uchino M., Turner M., 2008, *MNRAS*, 385, L108
- Risaliti G., Elvis M., Gilli R., Salvati M., 2003, *ApJ*, 587, L9
- Sabra B. M., Hamann F., 2001, *ApJ*, 563, 555
- Schartel N., Rodríguez-Pascual P. M., Santos-Lleó M., Ballo L., Clavel J., Guainazzi M., Jiménez-Bailón E., Piconcelli E., 2007, *A&A*, 474, 431 (S07)
- Schartel N., Rodríguez-Pascual P. M., Santos-Lleó M., Jiménez-Bailón E., Ballo L., Piconcelli E., 2010, *A&A*, 512, A75
- Schmidt M., Green R. F., 1983, *ApJ*, 269, 352
- Shi Y., et al., 2007, *ApJ*, 669, 841
- Strüder L., et al., 2001, *A&A*, 365, L18
- Turner M. J. L., et al., 2001, *A&A*, 365, L27
- Véron-Cetty M.-P., Véron P., 2010, *A&A*, 518, A10
- Young S., Axon D. J., Robinson A., Hough J. H., Smith J. E., 2007, *Natur*, 450, 74
- Zdziarski A. A., Gierliński M., 2004, *PThPS*, 155, 99